Biocatalysis and Agricultural Biotechnology 50 (2023) 102709

Contents lists available at ScienceDirect

Biocatalysis and Agricultural Biotechnology

journal homepage: www.elsevier.com/locate/bab

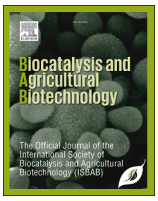

Recycling waste by manufacturing biomaterial for environmental engineering: Application to dye removal

Imane Akkari [a, **], Zahra Graba [a], Marta Pazos [b, *], Nacer Bezzi [a], Fatiha Atmani [c], Amar Manseri [d], Mohamed Mehdi Kaci [c, ***]

[a] Materials Technology and Process Engineering Laboratory (LTMGP), University of Bejaia, 06000, Bejaia, Algeria
[b] CINTEXT-Universidade de Vigo, Department of Chemical Engineering Campus As Lagoas-Marcosende, University of Vigo, 36310, Vigo, Spain
[c] Laboratory of Reaction Engineering, Faculty of Mechanical and Process Engineering (USTHB), BP 32, 16111, Algiers, Algeria
[d] Research Center of Semi-conductor Technology for Energy, CRTSE-02, Bd.Dr. Frantz FANON, B.P.140, Algiers, 7, Merveilles, 16038, Algeria

ARTICLE INFO

Handling Editor: Dr. Ching Hou

Keywords:
Activated hydrochar
Pomegranate peels
Adsorption
Basic red 46

ABSTRACT

There are several disposal and governance difficulties due to rapid bio-waste growth. Therefore, recycling and repurposing them for environmental purposes is garnering increasing attention. Hydrothermal carbonization (HTC) followed by phosphoric acid activation was used in this investigation to synthesize a novel activated hydrochar (AHPP) from pomegranate peels. X-Ray Diffraction, Fourier-transform infrared spectroscopy, Scanning electron microscopy with energy dispersive X-ray spectroscopy, Brunauer, Emmett and Teller (BET) surface area analysis and Barrett-Joyner-Halenda (BJH) pore size distribution, and pH of zero charge were exploited to define the characteristics of AHPP, which was then used to assess the uptake of Basic Red 46 (BR46) dye in the batch mode. Isothermal and kinetic investigations were accomplished with pH = 6, 0.5 $g.L^{-1}$ of adsorbent, 400 rpm at 298 K upon 60 min. The Freundlich model accurately presented the equilibrium curves with an adsorption capacity of 998.95 mg g^{-1}, while the PSO kinetic model adequately corresponded to the experimental data. Furthermore, thermodynamic data disclosed that the process was spontaneous, endothermic, and linked to a growing disorder at the adsorbent-adsorbate interface. Lastly, the reuse investigation using HCl ascertained that AHPP might be recycled ten times, whereas a probable adsorption mechanism was proffered. Overall, it is possible to conclude that activated hydrochar generated from pomegranate peels as cost-effective waste could be employed as an alternative sorbent in dining substantial effluents retaining BR46.

1. Introduction

Textile dyeing manufacturing is renowned as an intricate industry, with potentially substantial water, energy, and chemical resource consumption while also yielding extensive quantities of unsafe effluents, which is why many researchers regard it as the world's multiple environmentally defiling industry (Graba et al., 2022). Because of their inability to biodegrade, carcinogenicity, and mutagenicity; synthetic dyes and their derivatives are among the considerable hazardous pollutants; endangering human health, aquatic life, and the ecosystem as a whole (Akkari et al., 2022a).

* Corresponding author.
** Corresponding author.
*** Corresponding author.
E-mail addresses: imane.akkari@univ-bejaia.dz (I. Akkari), mcurras@uvigo.es (M. Pazos), mkaci@usthb.dz (M.M. Kaci).

https://doi.org/10.1016/j.bcab.2023.102709
Received 27 February 2023; Received in revised form 9 April 2023; Accepted 19 April 2023
Available online 20 April 2023

Azo cationic dyes like Basic Red 46 are among the extensively utilized in textile manufacturing; as a result, there was a greater focus on adequately managing them. Before being released, industrial effluents containing dyes may be treated using various techniques. These include biological techniques such as aerobic/anaerobic treatment (Shoukat et al., 2019), chemical techniques like redox treatment, precipitation, and photocatalysis (Kaci et al., 2021, 2022), and physical techniques such as adsorption, ion exchange, and membrane filtering (Atmani et al., 2022). Due to its simplicity, ease of utilization and excellent efficacy, adsorption is one of the most alluring and adaptable treatment modalities. Therefore, it is crucial to create novel adsorbents with high adsorption capacities, low investment costs, and superior renewability for removing dyes.

Under subcritical water conditions, low oxygen, 180–250 °C, and saturated pressure, biomass may undergo a thermochemical transformation into hydrochar, a high added value carbonaceous material. Hydrothermal carbonization means this action (HTC) (Román et al., 2018a). Dehydration, decarboxylation, condensation, polymerization, and aromatization are all involved in hydrochar creation. Unfortunately, a thorough understanding of the response mechanism is lacking (Funke and Ziegler, 2010). HTC's technology has quick, secure, affordable, and valuable processing advantages. A good carbon range, porous nature, many oxygenated functional groups on the surface, low moisture content, and chemical and biological resistance are all characteristics of the generated hydrochar. However, its modest surface area and pore volume may occasionally restrict its adsorption effectiveness (Yu et al., 2020). So, activating hydrochar could improve its surface characteristics and adsorption potential. Additionally, the use of hydrochar as a precursor for the preparation of porous carbonaceous materials (activated hydrochars, for example) has shown promise (El Hadrami et al., 2022).

Lower activation temperatures, greater gains, and well-developed porosity are just a few advantages of chemical activation. Compared to other chemical agents, phosphoric acid shows more advantages, such as higher mass production, non-toxic characteristics and requires washing with water only (Yahya et al., 2015). The physicochemical characteristics of hydrochar can be enhanced by the introduction of acids. The additional acid may catalyze the hydrolysis reaction, which increases hydrochar's active surface area and functional groups (Braghiroli et al., 2015). It has been noted that adding phosphoric acid could promote the production of hydrochar's high surface areas and acidic functional groups (Zhou et al., 2017; Liu et al., 2018). In order to increase the adsorption capacity, activation using phosphoric acid appears to be highly prospective.

Pomegranates are easily found in the region, and the peels are a cheap byproduct. Promising results came from their investigation as a biosorbent (Akkari et al., 2021). However, its limited textural properties limit its performance. Therefore, it seems convenient to value pomegranate peels to produce hydrochar-based adsorbents to eliminate water contaminants. Yet, no earlier study investigated removing Basic Red 46 (BR46) on activated hydrochar yielded with pomegranate peels, which is important.

This study centred on making a new phosphoric acid-activated hydrochar from pomegranate peels. The produced powder was then characterized through diverse approaches for removing BR46. Working parameters affecting the process were optimized, while the isothermal, kinetic, and thermodynamic investigations were checked. Last, the viability of recycling prepared adsorbent was explored, and the plausible mechanism was also suggested.

2. Experimental part

2.1. Preparation of dye solution

Molecular dimensions of BR46, its molecular electrostatic potential surfaces and the HOMO-LUMO orbitals are shown in Fig. 1. Full details of the calculation and preparation of BR46 solutions are given in Section 1 of Supplementary Material.

2.2. Preparation of activated hydrochar

100 mL of distilled water was soaked for 2 h with 10 g of powdered pomegranate peels (PPR). After that, the mixture was put into an autoclave created of stainless steel, and hydrothermal carbonization (HTC) was brought out at 220 °C for 20 h under autogenously heating. These operating parameters were selected following previous hydrochar production techniques using agricultural byproducts documented in the literature (Román et al., 2018b). The powder was then quickly chilled to room temperature, and the hydrochar (HCPP) was collected, cleaned, and dried for an entire night at 100 °C.

The activation process was performed using phosphoric acid solution mixed with HCPP in a 4:1 H_3PO_4/HCPP weight ratio, obeyed by calcination (600 °C, 1 h) under N_2 atmosphere, per the methodology outlined in detail formerly (Fernandez et al., 2015). The generated activated hydrochar (AHPP) was then dried, powdered, sieved (<100 μm) with a moderate particle size of 18.99 nm (Table 1), and kept in a desiccator until it was needed. Note that ACPP is an adsorbent prepared by the same procedure of activating pomegranate peels by phosphoric acid but without combining with HTC (Akkari et al., 2022a). Some characteristics of the mentioned adsorbents based on pomegranate peels are gathered in Table 1.

2.3. Characterization of activated hydrochar

The activated hydrochar (AHPP) was characterized through X-Ray Diffraction, Fourier-transform infrared spectroscopy, Scanning electron microscopy with energy dispersive X-ray spectroscopy, BET surface area analysis and BJH pore size distribution, and pH of zero charge. This section is detailed in Supplementary Material (section 2).

2.4. Adsorption experiments

While analyzing the experimental conditions ($C_0 = 200$ mg.L^{-1} for 60 min), adsorption tests were carried out using a beaker containing a volume of the solution. At ideal conditions of batch adsorption (pH 6, 0.5 g.L^{-1} of AHPP, 400 rpm at 25 °C), the effects of duration, starting dye concentration, isotherms, kinetics, thermodynamics and reuse of AHPP have been examined.

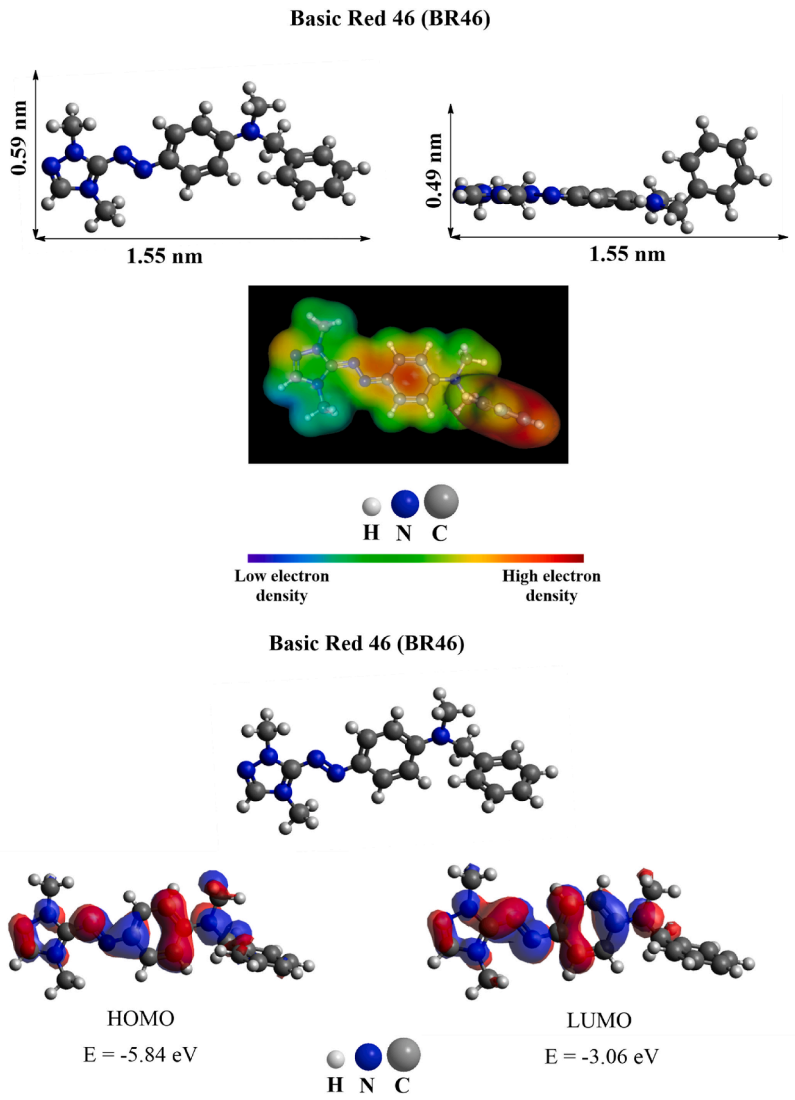

Fig. 1. Molecular dimensions of BR46 dye ($C_{18}H_{21}N_6O_4S$), its molecular electrostatic potential surfaces and the HOMO-LUMO orbitals.

Table 1
Comparaison of AHPP's characteristics with previously developed pomegranate peel adsorbents.

Parameter	This study	Akkari et al. (2022a)	Akkari et al. (2023)	Akkari et al. (2021)
	AHPP	ACPP	HCPP	PPR
C (wt. %)	62.76	61.23	65.4	30.6
O (wt. %)	30.78	30.69	28.2	61.7
P (wt. %)	6.46	8.09	–	–
Average particle size (nm)	18.998	58.784	–	–
BET surface area ($m^2.g^{-1}$)	315.812	102.068	5.008	1.046
Total pore volume ($cm^3.g^{-1}$)	0.397	0.069	0.023	0.001
Adsorption average pore size (4V/A by BET) (nm)	5.032	2.724	–	–
BJH Adsorption average pore size (nm)	6.479	3.595	–	6.012
pH_{PZC}	2.42	2.31	5.47	6.87

The specimens were centrifuged (6000 rpm; 10 min), C_t and C_e were quantified via a UV–Vis Spectrophotometer (SHIMADZU UV-1800) at λ_{max} (531 nm).

The adsorption uptake (q) and removal rate (R) are figured utilizing equations (1) and (2):

$$q_{(e,t)} = \frac{(C_0 - C_{(e,t)})\ V}{M} \tag{1}$$

$$R_{(e,t)} = \frac{(C_0 - C_{(e,t)})}{C_0} \times 100 \tag{2}$$

C_o ($mg.L^{-1}$) denotes BR46 concentration at t = 0, C_e and C_t ($mg.L^{-1}$) express, respectively, BR46 concentrations at the equilibrium and at time t, V (L) is the solution's volume, and M (g) is AHPP's mass.

Varied isotherm models, along with Langmuir, Freundlich and Temkin, allow for examining the interactions of BR46 with AHPP surface (Langmuir, 1918; Freundlich, 1906; Temkin and Pyzhev, 1940). These are presented in Equations (3)–(5):

$$q_e = \frac{q_m K_L C_e}{1 + K_L C_e} \tag{3}$$

$$q_e = K_F.\ C_e^{1/n} \tag{4}$$

$$q_e = B\ln(AC_e) \tag{5}$$

q_e ($mg.g^{-1}$) defines the uptake at equilibrium, the final BR46 concentration is C_e ($mg.L^{-1}$), q_m ($mg.g^{-1}$) is the monolayer adsorption capacity, K_L ($L.mg^{-1}$) and K_F are the Langmuir and Freundlich constants, n stands the adsorption intensity, A implies the Temkin isotherm constant ($L.mg^{-1}$), and B stands Temkin adsorption heat constant ($J.mol^{-1}$).

To depict the reaction sequence of the BR46 adsorption over AHPP, pseudo-first order (PFO) and pseudo-second order (PSO) models (Lagergren, 1898; Ho and McKay, 1999)] have been examined. These models are yielded by formulas (6) and (7), including both:

$$q_t = q_e\left(1 - e^{-k_1 t}\right) \tag{6}$$

$$q_t = \frac{k_2 q_e^2 t}{1 + k_2 q_e t} \tag{7}$$

q_t and q_e express the quantity of BR46 ($mg.g^{-1}$) adsorbed respectively at a time and equilibrium, k_1 and k_2 represent the rate constants of the PFO and The PSO.

The kinetic and equilibrium models were discussed using determination coefficient values (R^2), Adj. R^2 and χ^2.

Understanding the procedure is made possible by the reckoning of thermodynamic grounds, including ΔG°, ΔH°, and ΔS° exploiting formulas (8) and (9):

$$\Delta G^\circ = -RT\ln K_e^0 \tag{8}$$

$$\ln\ K_e^0 = \frac{\Delta S^\circ}{R} - \frac{\Delta H^\circ}{RT} \tag{9}$$

K_e^0 stands for the dimensionless thermodynamic equilibrium constant (Zanella et al., 2021; Lima et al., 2019), R represents the constant of gases, and T (K) tells the absolute temperature.

3. Results and discussion

3.1. Characterization

AHPP X-Ray Diffraction (XRD) pattern is seen in Fig. 2. The large peaks at (002) and (100) at 25° and 44° indicate its amorphous structure (Wang et al., 2021).

Fig. 3 depicts the results of Fourier-transform infrared spectroscopy (FTIR) characterization abused to quantify functional groups. The broad band at approximately 3293 cm^{-1} is credited to N–H and/or O–H stretching vibrations, whereas the peaks at 2924 and 2853 cm^{-1} are attributed to C–H asymmetric stretching vibrations in CH_2 groups (Liu et al., 2017). The peak at 1744 cm^{-1} is directly related to C = O, and the CN stretching/NH bending modes may be connected to the peak at 1615 cm^{-1} (Baláž et al., 2016). C = C in aromatic rings is associated with a 1425 cm^{-1} peak, while the peak at 1097 cm^{-1} may be from P–O–C reflecting the interaction of pomegranate peel surface with phosphoric acid (Bagheri et al., 2020). C–O, C–N, and C–O–C vibrations can be set to peaks ranging from 1023 to 1236 cm^{-1}, and the peaks at 534 cm^{-1} could stand due to C–H deformation. A summary of the prominent FTIR peaks of AHPP and their identification is given in Table 2. It is possible to conclude that the surface of AHPP is densely packed with functional groups, which can interact in different ways with the molecules of BR46.

Fig. 4(a–d) shows Scanning Electron Microscopy (SEM) pictures of AHPP material at various magnifications. An uneven particle way and a rugged, contrasting, and porous surface varying from 12.7 to 30 nm with a moderate diameter of 20.2 nm may be observed (Fig. 4 (f)), suggesting a convenient surface for the uptake of BR46. Energy Dispersive X-ray spectroscopy (EDS) was em-

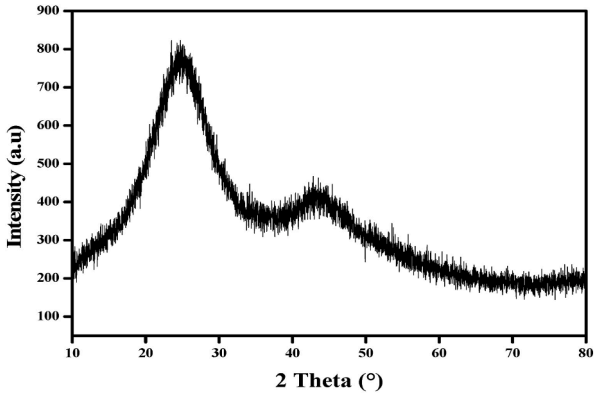

Fig. 2. XRD pattern of AHPP.

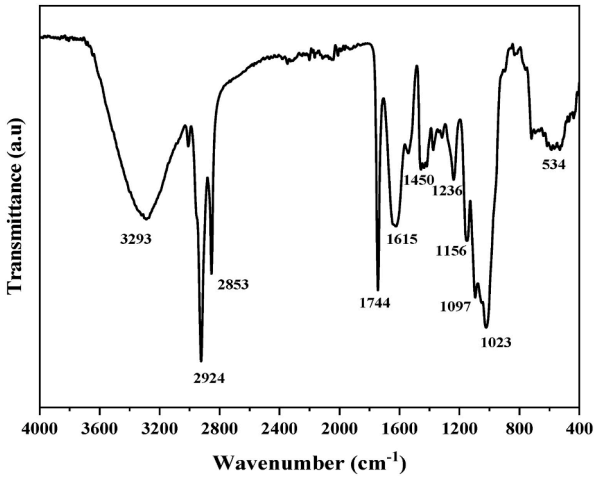

Fig. 3. FTIR Spectrum of AHPP.

Table 2
Identification of the main FTIR peaks of AHPP.

Wavenumber (cm^{-1})	Attribution
3293	–N–H and –O–H
2924 and 2853	C–H
1744	C = O
1615	C–N/N–H
1425	C = C in aromatic rings
1236, 1156 and 1023	C–O, C–N and C–O–C
1097	P–O–C
534	C–H

ployed to identify the composition of AHPP. Data Spectrum in Fig. 4 (e) and Table 1 demonstrates that the sample has high carbon content (62.76%). The presence of the element phosphorus is directly connected to phosphoric acid activation (H_3PO_4) (Han et al., 2020).

Fig. 5 displays textural analysis of AHPP. According to IUPAC classifications, the sample's nitrogen adsorption isotherm was classed as type IV, indicating a mesopores material (Tu et al., 2021). It should be pointed out that the medium BJH pore dimension of the adsorbent was equal to 6.47 nm (Table 1), while the molecular dimensions of the adsorbate are small likened to the pore dimensions of the adsorbent. For example, the BR46 dye has (1.55 × 0.59 × 0.49) nm as its molecular dimensions (Fig. 1), which shows that it could readily access AHPP pores. As indicated in Table 1, BET surface area and total pore volume of AHPP (315.812 $m^2\ g^{-1}$ and 0.397 $cm^3\ g^{-1}$) were considerably greater than those of previously developed pomegranate peel adsorbents; this demonstrates the efficiency of combining the HTC approach with phosphoric acid activation in the development of material textural qualities.

The pH of the zero charge (pH_{PZC}) is highly useful for determining the surface charge of adsorbents. When pH = pH_{PZC}, AHPP is electrically neutral. AHPP is positively charged with a pH < pH_{PZC} due to the protonation of surface functional groups, promoting anionic species adsorption. Alternatively, a pH > pH_{PZC} results in an overall negatively charged surface with deprotonated functional

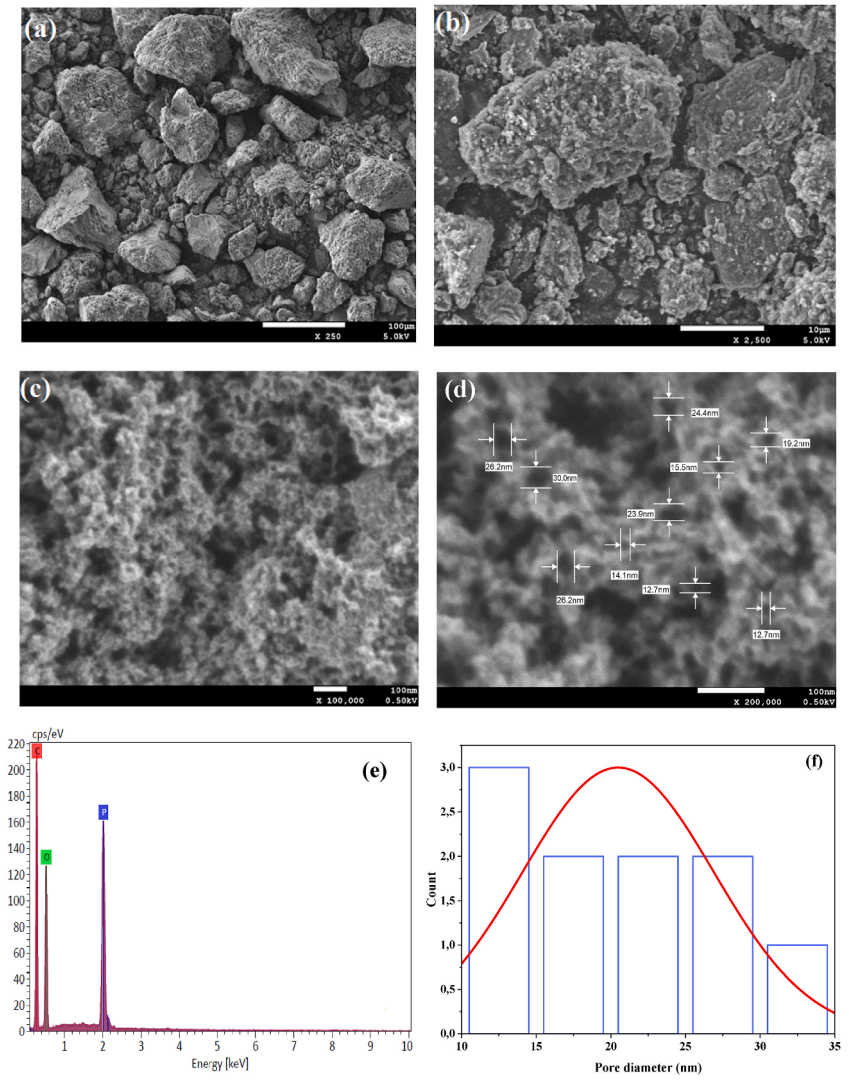

Fig. 4. SEM image at different magnifications (a–d), EDS Spectrum of AHPP (e) and porous size distribution histogram (f).

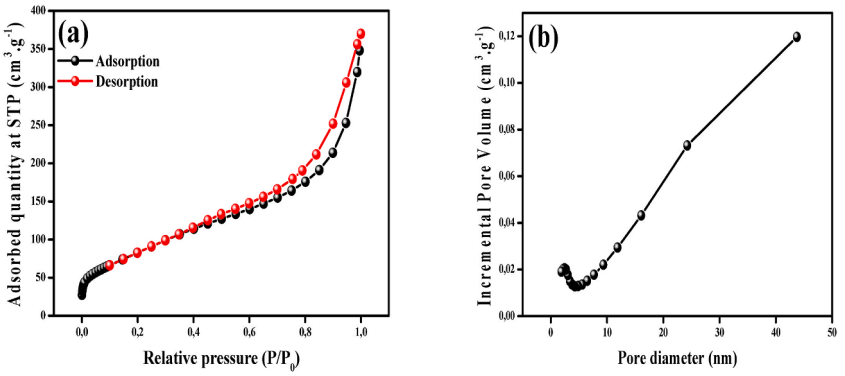

Fig. 5. N_2 adsorption/desorption isotherm of AHPP at 77 K (a) and BJH pore size distribution (b).

groups, which is favourable for catching cations (Liu et al., 2021). The pH_{PZC} of AHPP is reported to be 2.42 (Fig. 6 and Table 1); its acidic behaviour might be related to the activation by phospohoric acid.

3.2. Adsorption parameters

pH: it is a crucial parameter, as it may have an impact on the adsorbent's surface electrical charges and the dye molecules' ionization. Fig. 7 (a) depicts the impact of pH (from 2 to 10) on BR46 adsorption onto the AHPP surface and the pH-dependent BR46 species distribution. While pH extended from 2 to 6, the uptake boosted from 153.76 (R = 76.88%) to 199.92 mg g^{-1} (R = 99.96%), subsequently it decreased. It can stand clarified by AHPP pH_{PZC} and BR46 pKa values. Because of the protonation of its functional groups, AHPP's surface acquires a positive charge at pH < pH_{PZC}, preventing BR46 cations from taking up by electrostatic repulsion. The number of OH^- ions in the solution increases as the pH rises, promoting deprotonation of AHPP's functional groups, enabling its surface to ripen negatively charged, attracting dye cations electrostatically, and boosting the uptake (Naushad et al., 2019). At higher pHs (pH > pka), an excessive quantity of OH^- encircles the dye molecule, preventing its uptake on the negatively charged surface of AHPP.

AHPP dosage: Fig. 7 (b) shows the impact of varying AHPP amount on the process performance. While AHPP concentration was increased (0.25–2 g.L^{-1}), the uptake decreased from 739 (R = 92.37%) to 99.96 mg g^{-1} (R = 99.96%) because specific adsorption sites are unsaturated. However, for greater adsorbent dosages, a larger surface area and more adsorption sites may also boost the removal rate (Bayuo et al., 2019). Adsorbent dosages > or = 0.5 g.L^{-1} resulted in a minor increase in uptakes.

Agitation speed: This impact (100–600 rpm) on BR46 adsorption is given in Fig. 7 (c). Adsorption quantity rose from 371.96 (R = 92.99%) to 399.83 mg g^{-1} (R = 99.95%) with increasing agitation (100–400 rpm) and subsequently declined, ensuring the sameness of the adsorbent particles and dye solution (Saxena et al., 2020). At agitation rates increase, vortices develop, and a cut of the adsorbent gets dumped on the flask walls, reducing the homogeneity of the mixture.

Temperature: Adsorption capabilities rose slightly with temperature from 399.83 to 399.91 mg g^{-1} (Fig. 7d). Adsorption increases as temperature rises, meaning an endothermic process. This indicates that irregularity increases during the process. Because water molecules are liberated due to molecular interaction between BR46 and the surface of AHPP, irregularity at this interface rises (Değermenci et al., 2019; Banaei et al., 2017).

Time and initial concentration of BR46: Equilibrium was scrutinized based on initial concentration of BR46 and time. Fig. 7 (e) depicts the adsorbed quantity q_t (mg.g^{-1}) with time (0–60 min) for varied starting BR46 concentrations (20–500 mg.L^{-1}). The findings indicated that for all examined concentrations, BR46 adsorption on the surface of AHPP is very high in the first minute and reaches equilibrium within 60 min. A substantial number of unoccupied uptake sites can be noticed at first, and this number eventually declines (Muinde et al., 2020). It was also shown that raising BR46 concentration (50–500 mg.L^{-1}) increased the adsorbed amount of BR46 (39.99–998.95 mg g^{-1}). This could be clarified by the greater concentration gradient, which is a driving factor in moving adsorbate molecules to active adsorption sites and overcoming mass transfer resistance (Jawad et al., 2020a).

3.3. Adsorption isotherms

Fig. 7 (f) illustrates the experimental data for adsorption, and the nonlinear fit of the isotherm models studied. The isotherm profile is of type L (Langmuir) according to the Giles classification (Giles et al., 1974), which assumes that the molecules are adsorbed horizontally onto the adsorbent surface with little contest with solvent molecules.

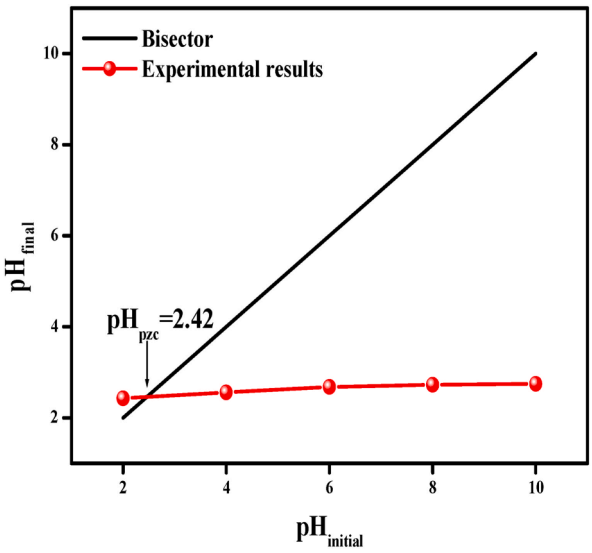

Fig. 6. pH_{pzc} of AHPP.

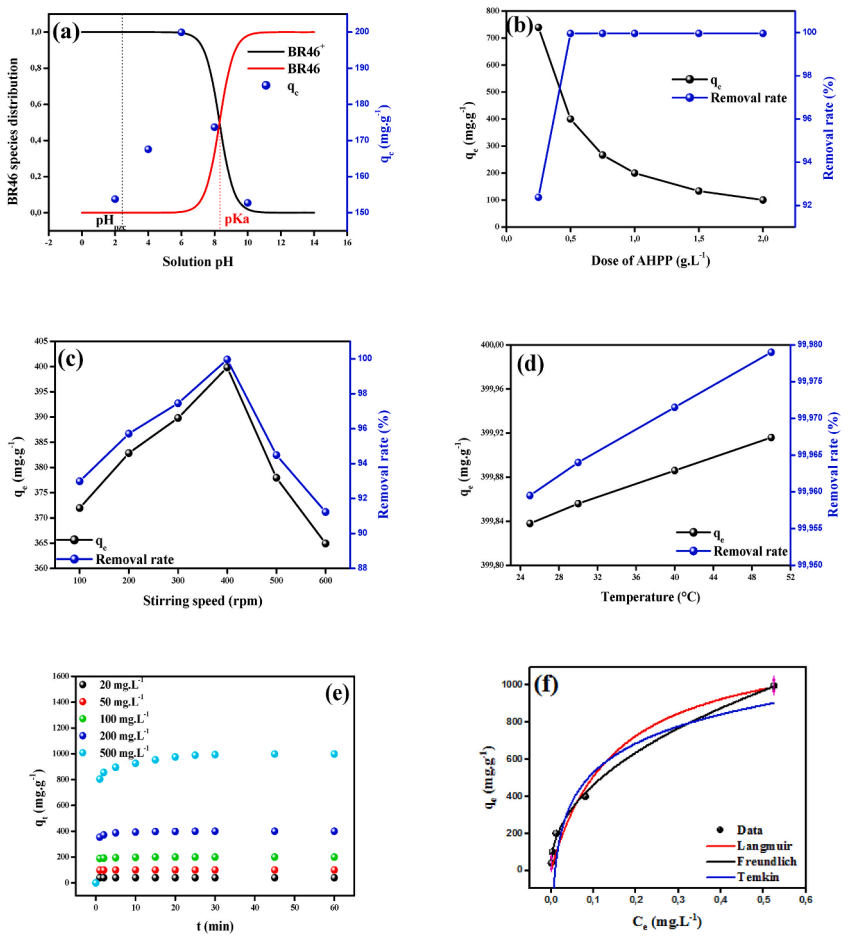

Fig. 7. The influence of different parameters on dye adsorption onto AHPP: solution pH (a), adsorbent dose (b), stirring speed (c), temperature (d) and contact time and initial dye concentration (e); and adsorption isotherm (f).

To better comprehend the process, Langmuir, Freundlich, and Temkin models suited the experimental findings. The results are given in Table 3.

Freundlich model had the highest R^2 and Adj. R^2 values and the lowest χ^2 value, demonstrating that it had the best match. This model covers the multilayer adsorption processes on heterogeneous surfaces with diverse adsorption strengths. As the active spots fill

Table 3
The values of parameters for each isotherm model used in the study.

Langmuir	q_m (mg.g^{-1})	1276.104
	K_L (L.mg^{-1})	6.614
	R^2	0.966
	Adj. R^2	0.955
	χ^2	6678.884
Freundlich	K_F	1339.549
	n	2.166
	1/n	0.461
	R^2	0.997
	Adj. R^2	0.996
	χ^2	466.005
Temkin	A (L.mg^{-1})	103.189
	B (J.mol^{-1})	226.853
	R^2	0.923
	Adj. R^2	0.923
	χ^2	3843.389

up more, the affinity forces weaken. There are a limited number of sites, and the most powerful are filled first (Syafiuddin et al., 2018).

According to the Freundlich model's heterogeneity factor (n), the process could be linear (n = 1), chemical (n < 1), or physical (n > 1). Additionally, cooperative adsorption and typical Langmuir isotherms are indicated by 1/n < 1 and 1/n > 1 (Foo and Hameed, 2010). The findings (Table 3) show that n and 1/n are 2.166 and 0.461, pointing to a physical process and favouring the standard Langmuir isotherm (Zanella et al., 2021).

3.4. Adsorption kinetics

The nonlinear fits are given in Fig. 8(a–e), and the estimated values are included in Table 4. Based on R^2, Adj. R^2 and χ^2 parameters, the PSO model provides the most suitable fit (Highest R^2 and Adj. R^2 values with the lowest values of χ^2). Additionally, the tight

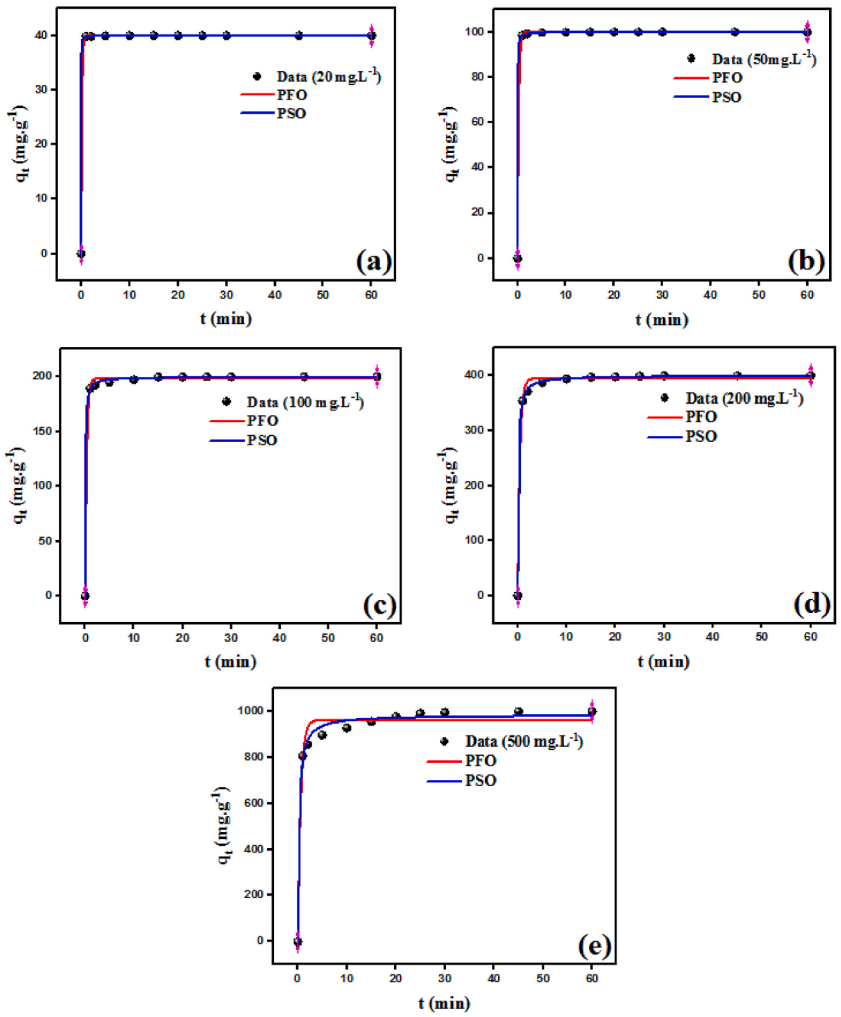

Fig. 8. Kinetic adsorption results for initial dye concentrations of 20 (a), 50 (b), 100 (c), 200 (d) and 500 mg.L^{-1} (e).

Table 4
Kinetic parameters.

Concentration (mg.L^{-1})	$q_{e\ exp}$ (mg.g^{-1})	Pseudo first-order kinetic					Pseudo second-order kinetic				
		$q_{e\ cal}$ (mg.g^{-1})	k_1 (min^{-1})	R^2	Adj. R^2	χ^2	$q_{e\ cal}$ (mg.g^{-1})	k_2 (g.mg $^{-1}$.min^{-1})	R^2	Adj. R^2	χ^2
20	39.998	39.973	5.612	0.999	0.999	0.002	39.999	4.980	1	1	4.981E-4
50	99.994	99.866	4.238	0.999	0.999	0.054	100.048	0.611	1	1	3.723E-4
100	199.976	198.323	3.029	0.998	0.998	6.903	199.766	0.079	0.999	0.999	1.579
200	399.838	395.129	2.173	0.996	0.995	57.646	400.406	0.018	0.999	0.999	2.895
500	998.95	960.636	1.656	0.980	0.978	1795.294	983.681	0.003	0.994	0.993	555.859

deal among the calculated and actual adsorption capacities (q_e) utilizing this model (Table 4) reveals that the PSO catches the uptake of BR46 on AHPP. The surface possesses many sorption sites, as evidenced by a good match of PSO. As a result, the initial BR46 concentration could be low in comparison to the sorption capacity of AHPP (Vithanage et al., 2016). Meanwhile, it may be asserted that the mechanism is caused not only by multilayer physical interactions but also by chemisorption (Jawad et al., 2020b).

3.5. Thermodynamic study

The thermodynamic parameters were established using ln K_e^0 versus 1/T plot (Fig. 9 and Table 5). $\Delta G^\circ < 0$ and the positive value of ΔH° (3.288E-06 kJ mol^{-1}) denote a spontaneous and endothermic process, while ΔH° magnitude < 40 kJ mol^{-1} implies that the adsorption process is physical (Tran et al., 2016). ΔS° (7.856E-05 kJ mol^{-1}.K^{-1}) defines the affinity of BR46 to the surface of AHPP, demonstrating that the dye molecules on the surface fast substitute the solvent molecules, enhancing the adsorption capacity (Ghibate et al., 2021).

3.6. Reuse study

The reuse scope of an adsorbent is directly proportional to its subsequent practical application. Details of this study are given in Supplementary Material (section 3). As illustrated in Fig. 10, after ten cycles, the adsorption capacity was nearly constant (998.95–969.14 mg g^{-1}). This validates AHPP's strong performance and implies that it might be suitable for water treatment applications.

Table 6 compares the adsorption capacity of BR46 onto AHPP to those of several adsorbents collected from the literature. AHPP demonstrated excellent performance with a remarkable uptake of 998.95 mg g^{-1} and an efficiency of 99.95%; affirming that the prepared activated hydrochar is promising and looks capable of removing a wide variety of contaminants. In addition, Table 7 compares the uptake of BR46 on the pomegranate peel-based adsorbents already studied and that of AHPP. It appears from these data that AHPP had the highest performance, and that the combination of HTC process and activation with phosphoric acid was successful.

3.7. Probable adsorption mechanism

The primary challenge for adsorption studies is to suggest plausible mechanisms to better comprehend all probable reactions/interactions throughout the process. In this context, different factors could play critical roles in the adsorption mechanism and must be considered, including the nature and complicatedness of the adsorbate structure, adsorbent surface characteristics and the adsorbent/adsorbate specific interactions.

Depending on BET analysis, the dimensions of the BR46 molecule is slighter than the pore size of AHPP, allowing it to infiltrate the substrate's microstructure easily. This may indicate that the adsorption mechanism can include pore-filling.

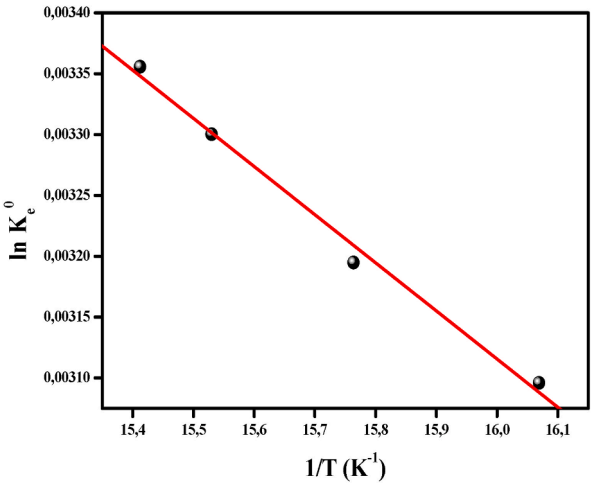

Fig. 9. Plot of Van't Hoff equation.

Table 5
Thermodynamic parameters at different temperatures.

T (K)	lnK_e^0	ΔG° (kJ.mol^{-1})	ΔH° (kJ.mol^{-1})	ΔS° (kJ.mol^{-1}.K^{-1})
298	15.412	−38.166	3.288E-06	7.856E-05
303	15.529	−39.103		
313	15.763	−41.001		
323	16.069	−43.131		

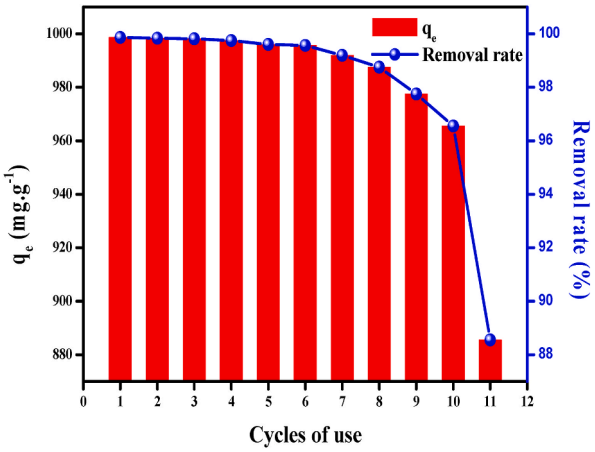

Fig. 10. Adsorption/desorption cycles of BR46 onto AHPP.

Table 6
Comparison of BR46 dye adsorption onto various adsorbents.

Adsorbent	Adsorption capacity (mg.g^{-1})	Reference
Synthesize graphene oxide nanoadsorbent	370.4	Shoushtarian et al. (2020)
Activated carbon from ziziphus lotus stones	307	Boudechiche et al. (2019)
Activated pine sawdust	312.5	Şentürk and Yıldız (2020)
Fe@graphite core-shell magnetic nanocomposite	46.7	Konicki et al. (2018)
Raw cactus fruit peel	82.58	Akkari et al. (2022b)
Activated clay	175	Mekatel et al. (2021)
Biochar prepared from *Chrysanthemum morifolium* Ramat straw	53.19	Yang et al. (2021)
Activated hydrochar from pomegranate peels	998.95	The present study

Table 7
Comparison of BR46 dye adsorption onto pomegranate peel adsorbents.

Adsorbent	Adsorption capacity (mg.g^{-1})	Preparation method	Particle size (μm)	Surface area (m^2.g^{-1})	pH	Adsorbent dose (g.L^{-1})	Initial BR46 concentration (mg.L^{-1})	Time (min)	T (°C)	Reference
Raw pomegranate peels (PPR)	86.13	Without any physical or chemical activation	<100	1.046	7	2	200	60	25	Akkari et al. (2021)
Hydrochar from pomegranate peels (HCPP)	367.72	Hydrothermal carbonization	<100	5.008	6	1.2	500	60	25	Akkari et al. (2023)
Activated carbon from pomegranate peels (ACPP)	551.58	Phosphorique acid activation	<100	102.068	6	0.8	500	60	25	Akkari et al. (2022a)
Phosphoric acid activated hydrochar from pomegranate peels (AHPP)	998.95	Hydrothermal carbonization + Phosphorique acid activation	<100	315.812		0.5	500	60	25	This study

The studies of isotherm and thermodynamic parameters conclude that multilayer physical sorption can manage the process. Meanwhile, the kinetic study revealed that physical sorption is not the only mean of adsorption but also chemisorption.

Considering the pH_{PZC} of AHPP and pKa of BR46, studying the solution pH impact on the uptake revealed that the process strongly depends on electrostatic interactions. That is why; the electrostatic draw among the negatively charged surface of AHPP and BR46 cations could be one of the crucial interactions in the adsorption mechanism.

Moreover, the results of FTIR exposed the fact of several functional groups of AHPP that can contribute to the adsorption of BR46 by other types of interactions besides electrostatic interactions:

- The dipole-dipole hydrogen sticking could ensue among the H-donor atom (nitrogen) in BR46 molecules and hydroxyl groups of AHPP (H-acceptor). In contrast, the Yoshida hydrogen bonding interactions (π-H bonding) may happen among the aromatic rings of BR46 and the hydroxyl groups on the AHPP surface (Dao et al., 2021).

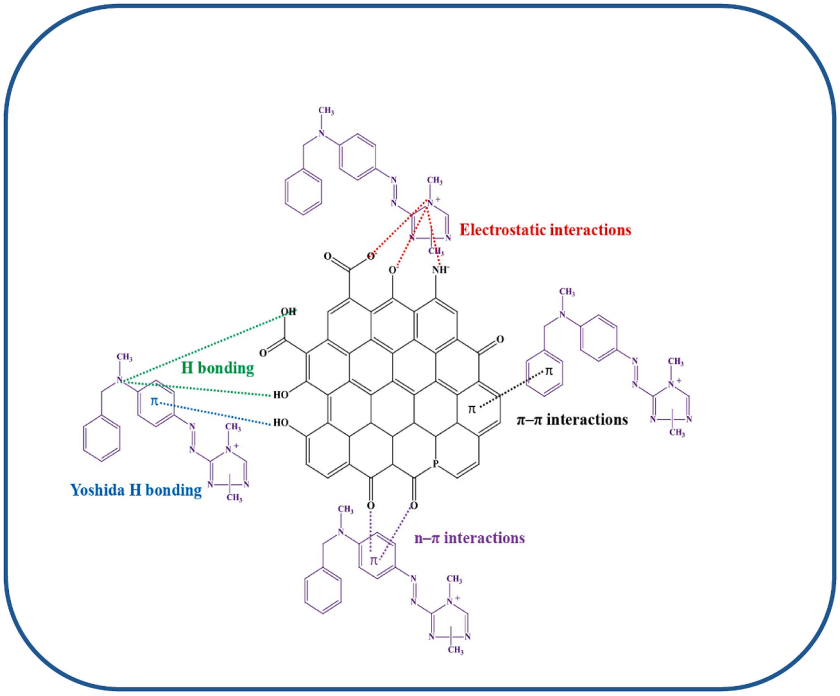

Fig. 11. Possible adsorption mechanism of BR46 over AHPP surface.

- π–π interactions may also occur between π aromatic rings donors of BR46 and π acceptor groups in the surface of the adsorbent (π electron system of AHPP) (Jawad et al., 2020c).
- In addition to that, another type of interaction may occur, probably n–π interactions between the oxygen groups onto AHPP (electron donors) and the aromatic rings of BR46 (electron acceptors) (Tran et al., 2017).

To sum up,Fig. 11illustrates the probable interactions between the BR46 molecule and the AHPP surface.

4. Conclusion

By combining the hydrothermal carbonization process and phosphoric acid activation, a novel adsorbent based on pomegranate peels (AHPP) was synthesized in this investigation. The features of AHPP were depicted through X-Ray Diffraction, Fourier-transform infrared spectroscopy, Scanning electron microscopy with energy dispersive X-ray spectroscopy, BET surface area analysis and BJH pore size distribution, and pH of zero charge, and the efficacy of combining the HTC method with H_3PO_4 activation in the improvement of adsorbent quality was demonstrated. At ideal operating conditions, BR46 dye batch adsorption experiments revealed an impressive uptake of 998.95 mg g^{-1} with a clearance rate of 99.95%. Freundlich and PSO models adequately modelled isotherms and kinetics, and adsorption was spontaneous and endothermic. Additionally, AHPP sustainability was scrutinized through recyclability screening for up to 10 successive runs without any noticeable defeat of effectiveness. Lastly, the adsorption mechanism of BR 46 over AHPP was also proposed. In closing, we assess the potential for valorizing pomegranate peels by designing a novel activated hydrochar, economical and eco-friendly for clearing BR46 and purifying textile wastewater.

Declaration of competing interest

The authors declare the following financial interests/personal relationships which may be considered as potential competing interests: The authors would like to thank the Algerian Ministry of High Education and the University of Bejaia for the financial support. Marta Pazos reports financial support was provided by Spain Ministry of Science and Innovation.

Data availability

Data will be made available on request.

Acknowledgments

The authors would like to thank the Algerian Ministry of High Education and the University of Bejaia for the financial support. This research has been supported Project PID2020-113667GBI00 funded by MCIN/AEI/10.13039/501100011033. Funding for open access charge: Universidade de Vigo/CISUG.

Appendix A. Supplementary data

Supplementary data to this article can be found online at https://doi.org/10.1016/j.bcab.2023.102709.

References

Akkari, I., Graba, Z., Bezzi, N., Vithanage, M., Kaci, M.M., 2022a. New insights into the effective removal of Basic Red 46 onto activated carbon produced from pomegranate peels. Biomass Conversion and Biorefinery 1–14.

Akkari, I., Graba, Z., Bezzi, N., Merzeg, F.A., Bait, N., Ferhati, A., 2021. Raw Pomegranate Peel as Promise Efficient Biosorbent for the Removal of Basic Red 46 Dye: Equilibrium, Kinetic, and Thermodynamic Studies. Biomass Conversion and Biorefinery, pp. 1–14.

Akkari, I., Graba, Z., Bezzi, N., Merzeg, F.A., Bait, N., Ferhati, A., Kaci, M.M., 2022b. Biosorption of Basic Red 46 Using Raw Cactus Fruit Peels: Equilibrium, Kinetic and Thermodynamic Studies. Biomass Conversion and Biorefinery, pp. 1–12.

Akkari, I., Spessato, L., Graba, Z., Bezzi, N., Kaci, M.M., 2023. A sustainably produced hydrochar from pomegranate peels for the purification of textile contaminants in an aqueous medium. Sustain. Chem. Pharm. 31, 100924.

Atmani, F., Kaci, M.M., Yeddou-Mezenner, N., Soukeur, A., Akkari, I., Navio, J.A., 2022. Insights into the Physicochemical Properties of Sugar Scum as a Sustainable Biosorbent Derived from Sugar Refinery Waste for Efficient Cationic Dye Removal. Biomass Conversion and Biorefinery, pp. 1–15.

Bagheri, A., Abu-Danso, E., Iqbal, J., Bhatnagar, A., 2020. Modified biochar from Moringa seed powder for the removal of diclofenac from aqueous solution. Environ. Sci. Pollut. Control Ser. 27 (7), 7318–7327.

Baláž, M., Ficeriová, J., Briančin, J., 2016. Influence of milling on the adsorption ability of eggshell waste. Chemosphere 146, 458–471.

Banaei, A., Samadi, S., Karimi, S., Vojoudi, H., Pourbasheer, E., Badiei, A., 2017. Synthesis of silica gel modified with 2, 2′-(hexane-1, 6-diylbis (oxy)) dibenzaldehyde as a new adsorbent for the removal of Reactive Yellow 84 and Reactive Blue 19 dyes from aqueous solutions: equilibrium and thermodynamic studies. Powder Technol. 319, 60–70.

Bayuo, J., Pelig-Ba, K.B., Abukari, M.A., 2019. Adsorptive removal of chromium (VI) from aqueous solution unto groundnut shell. Appl. Water Sci. 9 (4), 1–11.

Boudechiche, N., Fares, M., Ouyahia, S., Yazid, H., Trari, M., Sadaoui, Z., 2019. Com-parative study on removal of two basic dyes in aqueous medium by adsorption using activated carbon from Ziziphus lotus stones. Microchem. J. 146, 1010–1018.

Braghiroli, F.L., Fierro, V., Parmentier, J., Vidal, L., Gadonneix, P., Celzard, A., 2015. Hydrothermal carbons produced from tannin by modification of the reaction medium: addition of H+ and Ag+. Ind. Crop. Prod. 77, 364–374.

Dao, M.U., Le, H.S., Hoang, H.Y., Tran, V.A., Doan, V.D., Le, T.T.N., Sirotkin, A., 2021. Natural core-shell structure activated carbon beads derived from Litsea glutinosa seeds for removal of methylene blue: facile preparation, characterization, and adsorption properties. Environ. Res. 198, 110481.

Değermenci, G.D., Değermenci, N., Ayvaoğlu, V., Durmaz, E., Çakır, D., Akan, E., 2019. Adsorption of reactive dyes on lignocellulosic waste; characterization, equilibrium, kinetic and thermodynamic studies. J. Clean. Prod. 225, 1220–1229.

El Hadrami, A., Ojala, S., Brahmi, R., 2022. Production of activated carbon with tunable porosity and surface chemistry via chemical activation of hydrochar with phosphoric acid under oxidizing atmosphere. Surface. Interfac. 30, 101849.

Fernandez, M.E., Ledesma, B., Román, S., Bonelli, P.R., Cukierman, A.L., 2015. Development and characterization of activated hydrochars from orange peels as potential adsorbents for emerging organic contaminants. Bioresour. Technol. 183, 221–228.

Foo, K.Y., Hameed, B.H., 2010. Insights into the modeling of adsorption isotherm systems. Chem. Eng. J. 156 (1), 2–10.

Freundlich, H.M.F., 1906. Over the adsorption in solution. J. Phys. Chem. 57, 1100–1107. 385471.

Funke, A., Ziegler, F., 2010. Hydrothermal carbonization of biomass: a summary and discussion of chemical mechanisms for process engineering. Biofuels, Bioproduct. Bioref. 4 (2), 160–177.

Ghibate, R., Senhaji, O., Taouil, R., 2021. Kinetic and thermodynamic approaches on Rhodamine B adsorption onto pomegranate peel. Case Studies in Chemical and Environmental Engineering 3, 100078.

Giles, C.H., Smith, D., Huitson, A., 1974. A general treatment and classification of the solute adsorption isotherm. I. Theoretical. J. Colloid Interface Sci. 47 (3), 755–765.

Graba, Z., Akkari, I., Bezzi, N., Kaci, M.M., 2022. Valorization of olive–pomace as a green sorbent to remove Basic Red 46 (BR46) dye from aqueous solution. Biomass Conversion and Biorefinery 1–12.

Han, Q., Wang, J., Goodman, B.A., Xie, J., Liu, Z., 2020. High adsorption of methylene blue by activated carbon prepared from phosphoric acid treated eucalyptus residue. Powder Technol. 366, 239–248.

Ho, Y.S., McKay, G., 1999. Pseudo-second order model for sorption processes. Process Biochem. 34 (5), 451–465.

Jawad, A.H., Mubarak, N.S.A., Abdulhameed, A.S., 2020a. Tunable Schiff's base-cross-linked chitosan composite for the removal of reactive red 120 dye: adsorption and mechanism study. Int. J. Biol. Macromol. 142, 732–741.

Jawad, A.H., Malek, N.N.A., Abdulhameed, A.S., Razuan, R., 2020b. Synthesis of magnetic chitosan-fly ash/Fe3O4 composite for adsorption of reactive orange 16 dye: optimization by Box–Behnken design. J. Polym. Environ. 28 (3), 1068–1082.

Jawad, A.H., Mohd Firdaus Hum, N.N., Abdulhameed, A.S., Mohd Ishak, M.A., 2020c. Mesoporous activated carbon from grass waste via H3PO4-activation for methylene blue dye removal: modelling, optimisation, and mechanism study. Int. J. Environ. Anal. Chem. 1–17.

Kaci, M.M., Nasrallah, N., Atmani, F., Kebir, M., Guernanou, R., Soukeur, A., Trari, M., 2021. Enhanced photocatalytic performance of CuAl2O4 nanoparticles spinel for dye degradation under visible light. Res. Chem. Intermed. 47 (9), 3785–3806.

Kaci, M.M., Nasrallah, N., Djaballah, A.M., Akkari, I., Belabed, C., Soukeur, A., et al., 2022. Insights into the optical and electrochemical features of CuAl2O4 nanoparticles and it use for methyl violet oxidation under sunlight exposure. Opt. Mater. 126, 112198.

Konicki, W., Hełminiak, A., Arabczyk, W., Mijowska, E., 2018. Adsorption of cationic dyes onto Fe@ graphite core–shell magnetic nanocomposite: equilibrium, kinetics and ther-modynamics. Chem. Eng. Res. Des. 129, 259–270.

Lagergren, S.K., 1898. About the theory of so-called adsorption of soluble substances. Sven. Vetenskapsakad. Handingarl 24, 1–39.

Langmuir, I., 1918. The adsorption of gases on plane surfaces of glass, mica and platinum. J. Am. Chem. Soc. 40 (9), 1361–1403.

Lima, E.C., Hosseini-Bandegharaei, A., Moreno-Piraján, J.C., Anastopoulos, I., 2019. A critical review of the estimation of the thermodynamic parameters on adsorption equilibria. Wrong use of equilibrium constant in the Van't Hoof equation for calculation of thermodynamic parameters of adsorption. J. Mol. Liq. 273, 425–434.

Liu, Y., Ma, S., Chen, J., 2018. A novel pyro-hydrochar via sequential carbonization of biomass waste: preparation, characterization and adsorption capacity. J. Clean. Prod. 176, 187–195.

Liu, M., Luo, G., Wang, Y., Xu, R., Wang, Y., He, W., Tan, J., Xing, M., Wu, J., 2017. Nano-silver-decorated microfibrous eggshell membrane: processing, cytotoxicity assessment and optimization, antibacterial activity and wound healing. Sci. Rep. 7 (1), 1–14.

Liu, Z.F., Liu, Z.J., Qie, L.M., Yao, Z.Y., 2021. Effects of melanin extraction on biosorption behavior of chestnut shells towards methylene blue. Water Conservat. Sci. Eng. 6 (3), 163–173.

Mekatel, E., Dahdouh, N., Sa-mira, A., Nibou, D., Trari, M., 2021. Removal of maxilon red dye by adsorption and photoca-talysis: optimum conditions, equilibrium, and kinetic studies. Iran. J. Chem. Chem. Eng. (Int. Engl. Ed.) 40 (1), 93–110.

Muinde, V.M., Onyari, J.M., Wamalwa, B., Wabomba, J.N., 2020. Adsorption of malachite green dye from aqueous solutions using mesoporous chitosan–zinc oxide composite material. Environ. Chem. Ecotoxicol. 2, 115–125.

Naushad, M., Alqadami, A.A., AlOthman, Z.A., Alsohaimi, I.H., Algamdi, M.S., Aldawsari, A.M., 2019. Adsorption kinetics, isotherm and reusability studies for the removal of cationic dye from aqueous medium using arginine modified activated carbon. J. Mol. Liq. 293, 111442.

Román, S., Libra, J., Berge, N., Sabio, E., Ro, K., Li, L., et al., 2018a. Hydrothermal carbonization: modeling, final properties design and applications: a review. Energies 11 (1), 216.

Román, S., Ledesma, B., Álvarez, A., Herdes, C., 2018b. Towards sustainable micro-pollutants' removal from wastewaters: caffeine solubility, self-diffusion and adsorption studies from aqueous solutions into hydrochars. Mol. Phys. 116 (15–16), 2129–2141.

Saxena, M., Sharma, N., Saxena, R., 2020. Highly efficient and rapid removal of a toxic dye: adsorption kinetics, isotherm, and mechanism studies on functionalized multiwalled carbon nanotubes. Surface. Interfac. 21, 100639.
Şentürk, İ., Yıldız, M.R., 2020. Highly efficient removal from aqueous solution by ad-sorption of Maxilon Red GRL dye using activated pine sawdust. Kor. J. Chem. Eng. 37 (6), 985–999.
Shoukat, R., Khan, S.J., Jamal, Y., 2019. Hybrid anaerobic-aerobic biological treatment for real textile wastewater. J. Water Process Eng. 29, 100804.
Shoushtarian, F., Moghaddam, M.R.A., Kowsari, E., 2020. Efficient regeneration/reuse of graphene oxide as a nanoadsor-bent for removing basic Red 46 from aqueous solutions. J. Mol. Liq. 312, 113386.
Syafiuddin, A., Salmiati, S., Jonbi, J., Fulazzaky, M.A., 2018. Application of the kinetic and isotherm models for better understanding of the behaviors of silver nanoparticles adsorption onto different adsorbents. J. Environ. Manag. 218, 59–70.
Temkin, M.J., Pyzhev, V., 1940. Recent Modifications to Langmuir Isotherms.
Tran, H.N., You, S.J., Chao, H.P., 2016. Thermodynamic parameters of cadmium adsorption onto orange peel calculated from various methods: a comparison study. J. Environ. Chem. Eng. 4 (3), 2671–2682.
Tran, H.N., You, S.J., Chao, H.P., 2017. Fast and efficient adsorption of methylene green 5 on activated carbon prepared from new chemical activation method. J. Environ. Manag. 188, 322–336.
Tu, W., Liu, Y., Xie, Z., Chen, M., Ma, L., Du, G., Zhu, M., 2021. A novel activation-hydrochar via hydrothermal carbonization and KOH activation of sewage sludge and coconut shell for biomass wastes: preparation, characterization and adsorption properties. J. Colloid Interface Sci. 593, 390–407.
Vithanage, M., Mayakaduwa, S.S., Herath, I., Ok, Y.S., Mohan, D., 2016. Kinetics, thermodynamics and mechanistic studies of carbofuran removal using biochars from tea waste and rice husks. Chemosphere 150, 781–789.
Wang, H., Li, Z., Yahyaoui, S., Hanafy, H., Seliem, M.K., Bonilla-Petriciolet, A., et al., 2021. Effective adsorption of dyes on an activated carbon prepared from carboxymethyl cellulose: experiments, characterization and advanced modelling. Chem. Eng. J. 417, 128116.
Yahya, M.A., Al-Qodah, Z., Ngah, C.Z., 2015. Agricultural bio-waste materials as potential sustainable precursors used for activated carbon production: a review. Renew. Sustain. Energy Rev. 46, 218–235.
Yang, X., Zhu, W., Song, Y., Zhuang, H., Tang, H., 2021. Removal of cationic dye BR46 by biochar prepared from Chrysanthemum morifolium Ramat straw: a study on adsorption equilibrium, kinetics and isotherm. J. Mol. Liq. 340, 116617.
Yu, X., Liu, S., Lin, G., Yang, Y., Zhang, S., Zhao, H., et al., 2020. KOH-activated hydrochar with engineered porosity as sustainable adsorbent for volatile organic compounds. Colloids Surf. A Physicochem. Eng. Asp. 588, 124372.
Zanella, H.G., Spessato, L., Lopes, G.K., Yokoyama, J.T., Silva, M.C., Souza, P.S., et al., 2021. Caffeine adsorption on activated biochar derived from macrophytes (Eichornia crassipes). J. Mol. Liq. 340, 117206.
Zhou, N., Chen, H., Feng, Q., Yao, D., Chen, H., Wang, H., et al., 2017. Effect of phosphoric acid on the surface properties and Pb (II) adsorption mechanisms of hydrochars prepared from fresh banana peels. J. Clean. Prod. 165, 221–230.